Master's Thesis

Sn-Pb-mixtures for Perovskite Solar Cells

TATNA: Engineering Nanoscience Nanomaterials

Ecóle Polytechnique Fédérale Lausanne, Laboratory of Photo Molecular Science

Lund Institute of Technology, Dept. Solid State Physics

Lund Institute of Technology, Dept. Chemical Physics

Author:	Fanny Baumann	fannybaumann9292@gmail.com
Supervisors:	Professor Anders Hagfeldt Head of Laboratory LSPM EPFL	Eva Unger Associate Professor Dept. of Chemical Physics Lund University
Assisting:	Bowen Yang Postdoc Senior Researcher LSPM EPFL	Sandy Sanchez Postdoc Senior Researcher LSPM EPFL
Examiner:	Magnus Borgström Professor Dept. of Solid State Physics Lund University	

LUNDS UNIVERSITET
Lunds Tekniska Högskola

Submitted on September 12, 2020

Abstract

Perovskite research has quickly gone from non-existent to one of the biggest reseach areas in Photovoltaics. There are still many questions to be solved regarding the stability, environmental impact, reproducible large area devices, efficiency and module fabrication cost of Perovskite Solar Cells, PSCs, before commercial up-scaling. Scientists all over the world are working towards solutions and over 15000 scientific articles were published from 2009 up until the end of 2019. Perovskite show great promise to fill the gap where Silicon Solar Cells fail today, such as inside charging for Internet Of Things and as active material in tunable bandgap tandem cells [1]. This master thesis focused on the fabrication of PSCs and the interchange of Lead, Pb, atoms with Tin, Sn, atoms in thin films and devices. Films with metal-organic-halide perovskite material Formamidinium(FA)LeadIodide, $FAPbI_3$ or FAPI, and different percentage of Sn were fabricated by several methods and investigated for an extended time period. We showed that different percentage of Sn in $FAPbI_3$ generated very different results regarding morphology, PhotoLuminescence(PL), photovoltaic performance, stablity and phase separation/segregation. The results give reasonable indications that Sn compositional engineering can be used to stabilize the otherwise unstable FAPbI, probably by changing bond lenghts in the Pb-I-Pb lattice to accommodate for strain and the non-symmetrical FA cation. It is also possible that increased stability and PL performance can arise from the creation of separate phases that add in stabilizing the strain build up by creating microscopical 3D structures as could be seen when samples were thoroughly investigated by Scanning Electron Microscopy and Confocal Microscopy. Standard PSC in this report reached a maximum of 19.5% Power Conversion Efficiency, PCE, and pin-structure Sn-Pb-mixed PSC with 60% Sn reached over 7% PCE and a short circuit current density, Jsc, over 21 mA/cm^2. Results indicated that the often used 50% Sn composition is not the most stable but that a choosing an alloy composition slightly off like 40% or 60% Sn for $FAPbSnI_3$ can be favorable to achieve higher efficiency and longer stability. Changing ratios subsequently lead to rises and falls in the connectivity in morphology, stability, intensity of PL and X-ray Diffraction spectra depending on the composition, something that is also discussed in regard to phase separations, strain, unit cell lattice/size and morphology.

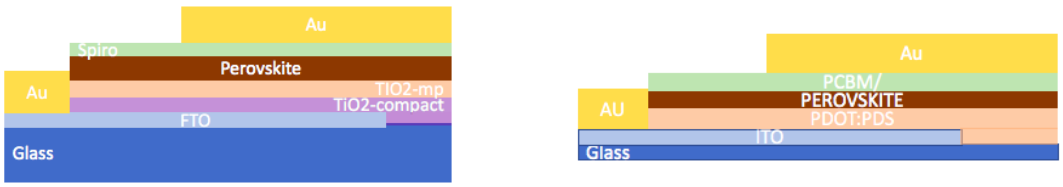

(a) normal n-i-p structure

(b) inverse p-i-n structure

Figure 1: Different bottom up layouts of PSCs.

keywords: *Perovskite Solar Cells, Compositional Engineering, Tin Lead, Thin film stability...*

Acknowledgments

This master's thesis work has been done as part of my Master of Science degree in Engineering Nanoscience at the Faculty of Engineering at Lund University. The project was executed at Laboratory of Photo Molecular Science, LSPM, at the Department of Chemistry at Ecóle Polytechnique Fédérale Lausanne, EPFL, Switzerland, autumn 2019 and January 2020. Report writing continued spring 2020 with throughout collaboration with Anders Hagfeldt's group at LSPM Lausanne.

I would like to thank Professor Anders Hagfeldt for the opportunity to pursue this project and for excellent insight into the photovoltaic field, his positive energy and fantastic setup at EPFL. I feel gratitude towards everyone at LSPM EPFL for making me feel welcome from the first day. I would like to give special thanks to some people for their collaboration and guidance, in no specific order. Postdoc Brian Carlsen for help with PhotoLuminescence, PL, and software analysis. Postdoc Bowen Yang for showing me the ropes around standard Perovskite Solar Cell, PSC, fabrication and the labs as well as project guidance. PhD Natalie Flores Dias for daily company, project guidance and inkjet collaboration. Postdoc Anwar Alanazi for interesting discussions about Formamidinuim, FA, perovskite structures. Postdoc Sandy Sanchez for excellent introduction to Flash Infra Red Annealing, FIRA, and collaborations, including letting me use the brand new setup at LSPM. Postdoc Jinno Hiroaki and Postdoc Hong Zhang for collaborations with Sn/Pb devices. Vicky Ling for collaboration on FIRA and daily discussions. My supervisor Doctor Eva Unger has been very valuable in giving me her analytic eye, hard sought energy and an excellent introduction to the field, she has an inspiring do-it-all attitude and as well as great vision for international collaborations. Professor Magnus Borgström has been very patient as my examiner during the project and I look forward to hearing his opinions on the report and presentation. Lina Ekstedt also had the privilege to work with Eva and Magnus, I would like to thank her for company in having simultaneous yet different projects but keeping track of each other. I would also like to present my gratitude towards the Helmholtz Zentrum Berlin, HZB, Quantsol Summer Camp for expanding my view of the Photovoltaic field and giving me an excellent warmup to the project. Finally I would like to thank Professor Sven Lidin for directing me towards this project, for connecting me to the correct people and for helping me find a great fit according to my interests and qualifications.

Needless to say I would also like to thank my family for their great patience and understanding during my studies and adventures since 2012. That including my wonderful fiancee for accommodating several changes in his lifestyle for me to pursue my passions for science and for using all his vacation time this year visiting me in Lund and Lausanne. Love you all. Finishing this work took a bit longer due to the pandemic crisis, spending the last months in the Spanish quarantine, thanks for understanding and I would like to hope all of you who read this report have come out ok.

Contents

List of Abbreviations

AM 1.5 G - Light simulated to represent sunlight at 1.5 air mass density arising from common angle of the sun towards the earth-surface, **CM** - Confocal Microscopy, **ETM** - Electron Transport Material, **EPFL** - Ecóle Polytechnique Fédérale Lausanne, **eV** - Electron Volt ($V * 1.602 * 10^{-}19$), **FF** - Fill Factor, **FIRA** - Firing Infrared Annealing, **HTM** - Hole Transport Material, **HZB** - Helmholtz Zentrum Berlin, **Jsc** - Short Circuit Current Density, **JV** - Current Density vs. Voltage, **LSPM** - Laboratory of Photo Molecular Science, **M** - Molar(concentration/mol), **mW** - milliWatt ($10^{-}3W$), **nip** - "normal" solar cell structure where n-extraction happens at the bottom, **nm** - Nanometer, **PCE** - Photon Conversion Efficiency, **pin** - "inverted" solar cell structure where the p-extraction is on the bottom, **PL** - Photo Luminescence, **PSC** - Perovskite Solar Cell, **rpm** - Revolutions per minute, **s** - second, **SEM** - Scanning Electron Microscopy, **SLG** - Soda Lime Glass, **SS-PL** - Steady State Photo Luminescence, **UV** - Ultra Violet light, **Voc** - Open Circuit Voltage, **wt%** - Weight percentage in solution, **XRD** - X-ray Diffraction, μ - Micro,

Chemical abbreviations

FTO - Fluorine doped Tin Oxide, **Zn powder** - Zink powder, **HCl** - Hydrochloric acid, **TiO2** - Titanium Dioxide, **O2** - Oxygen gas, **Acetyl Acetone** - 2,4-pentandion, **TTDIP** - Titanium Diisopropoxide, **IPA** - Isopropanol, **N2** - Nitrogen gas, **CB** - Chlorobenzene, **Spiro**-spiroMeOTAD(2,2′,7,7′-tetrakis-(N,N-di-4-methoxyphenylamino)-9,9′-spirobifluorene), **LiTFSI** - Lithium bis-trifluoromethanesulfonimide, **ACN** - Acetonitrile, **TBP** - Tributyl phosphate, **Au** - Gold, **DMF** - Dimethylformamide, **DMSO** - Dimethylsulfoxide, **FAI** - Formamidinium Iodide, **FA** - Formamidinium Cation, **MAPI** - Methylammonium Cation Lead Iodide Perovskite, **%Sn** - percentage of Tin in the Lead lattice of Perovskite, **PbI2** - Lead Iodide, **SnI2** - Tin Iodide, **FAPI** - Formamidinium lead iodide Perovskite, **FAPSI** - Formamidinium lead-tin iodide Perovskite,

Introduction

1.1 The Perovskite research field

The Perovskite research field Currently used Silicon Solar Cells, Si-SC, have a theoretical limit of efficiency in photon harvesting because of it's structural properties, Auger recombination and semiconductor band-gap, light below a certain wavelength cannot be absorbed and light above certain wavelengths lead to thermal losses [2] [3]. Perovskites show great promise as the material converts high energy photons to electrical energy efficiently and at the same time is more defect tolerant and easy to produce than Si-SC. Still, great efforts of the scientific community are needed to optimize the material if it should enter the photovoltaic market as a prominent alternative. As an introduction to the efforts of perovskite research the following is a short text about some applications of tunable band-gap perovskites, issues with Pb in perovskite and a short review of recent efforts with mixed-Pb/Sn perovskites.

Perovskite materials show good photovoltaic properties and at the same time a phenomenal tolerance for the exchange of elements within the structure, something that is proven to result in a tunable band-gap [4]. Fabricated Perovskite Solar Cells(PSC) can have a band-gap around 1.7 eV but also as low as around 1.22 eV, making them ideal for creating tandem structures with several active layers on top of each other. The tandem method allow bottom layers to absorb light that was transmitted through the top layers [4] and by this way Perovskite Solar Cells(PSCs) can produce highly efficient solar cells with a higher theoretical limit for photoelectric conversion than Si [1]. Increasing the efficiency would decrease total module cost for solar cells and increasing the application areas where they can be used. Even more interesting is that perovskite is fabricated directly from solution, making it possible to produce roll to roll perovskite solar cells, some cells with this format are already on the market today [1]. The crystal structure of perovskite allows

for a good charge separation once carriers are generated, and the crystal can be created by simple coating and heating. Perovskite is incorporated into the SC either alone or as part of a tandem cell. A tandem, or multijunction, cell includes two different active layers with different band-gaps so that a higher percentage of the light can be absorbed. Since perovskite atoms can be exchanged to form slightly different chemical compositions and in that way has a modifiable band-gap, the future of making tandem cells either together with Si or with another perovskite layer looks promising [5]. By exchanging atoms in the perovskite matrix the band gap of a perovskite can be optimized, and certain combinations show higher stability, efficiency and compatibility in different structures. It is not fully understood how the atom ratios of perovskite relates to these parameters and the structure of the material.

One issue in the PSC field is the high usage of lead and dangerous solvents during production. EU regulations regarding lead content in consumer products are tough, and the market steadily moves towards more lead free solar panels [1]. Removing part of the lead in the active layer of PSC would maybe contribute to greater acceptance on the market, and studying the solvent effects for crystallization is relevant for any field to achieve as safe and environmentally friendly production as possible. Many studies have shown that the perovskite recipe is crucial for stability and life-time of the active layer in PSC, another aspect important to the environmental impact of PSC production [6] [7] [].

That leads to the area of mixing the metal atom in Perovskite, previously the Pb atom has not been exchanged as frequently as other atoms in the perovskite matrix, but recent efforts have shown interesting results.

Many encountered PSCs with mixed metal-halide perovskites use pin-stacking layout [8]. One example is Qiaolei Han et al. [9], they achieved 17% PCE and high Jsc of 31 mA/cm^2 from $Cs_{0.1}MA_{0.2}FA_{0.7}Pb_{0.5}Sn_{0.5}I_3$ perovskite with a low bandgap that could maintain 95% stability over 102 days. The ability to lower the band gap by incorporating Sn atoms in the perovskite lattice also shows great promise for the fabrication of Perovskite-Perovskite tandem solar cells. Zhibin Yang et al. [10] created once again 50% Sn structure perovskite with $FA_{0.6}Cs_{0.4}Pb(I_{0.65}Br_{0.35})_3$ and $FA_{0.5}MA_{0.45}Cs_{0.5}Pb_{0.5}Sn_{0.5}I_3$, reaching 22.7% PCE with their record tandem cell based on pin-stacking with a recombination layer in the middle. The Sn-based single junction had a band-gap of 1.22 eV and average PCE of 19.4% [10]. Questions arise if it for future applications would be better to avoid incorporating many different components in the crystal lattice of the perovskite layer. Greater understanding of effects created in the structure might lead to better optimization of ratios used in recipes and through that maybe a reduction in chemical use such as anti-

solvents and rare element addition, which might help in up-scaling of production and fulfilling environmental and safety standards. It would be useful to understand exactly how the variation of atoms in the lattice contribute to stability, band-gap and electronic effects, not only for the performance of the active layer but to create successful band alignment between layers [11] [12] with adequate thickness to reduce degradation. Yang et al. [10] did simultaneous compositional engineering of the cation, the metal atom and the halide anions. A more simplistic approach will be used in this work as the goal is not to achieve the highest efficiency but to attain a more comprehensive understanding of the effect when interchanging the metal atoms. Most papers that aim for high efficiency today use "anti-solvent method" meaning that a quenching of the crystallization process leads to small but highly crystalline grains with a flat morphology. Angmo et al. [6] has done a detailed study of the use of anit-solvent and the correlation between film morphology, stability and photovoltaic efficiency.

Many articles today in the PSC research field focus on solar cell device optimization to reach high efficiency and find some understanding along the way. This report takes another approach and studies the efficiency as only one of the parameters regarding how the properties change with varying the metal atoms. In this exploratory study we hoped to gain insights leading to deeper understanding about processes occurring with compositional changes, specifically regarding the structure of the material and photoelectric effects.

1.2 Problem Description

Reducing lead content of perovskite and increasing the stability of high quality thin films are crucial issues that need to be solved to prepare Perovskite Solar Cells(PSC) for commercial use. More PSC research is needed.

1.3 Aim

Gaining understanding about PSC by attempts to produce high efficiency solar cells by standard perovskite fabrication. Investigating the effects of changing perovskite material Pb atoms for Sn atoms, general differences for different compositions, and the effects on stability and photovoltaic performance.

Theory

2.1 Physical and Chemical Concepts for Perovskite Solar Cells

2.1.1 Photovoltaics

The reason for carrier generation in semiconductors arises from excitation of an electron-hole pair at the event of photon absorption. Photons with energy corresponding to the band-gap(Eg) or slightly higher can be absorbed and transfer an electron from the valence band to the conduction band. In physical terms it is sometimes imagined that the electron and hole are transferred into different available positions in the crystal lattice. One of the most important factors for photovoltaic performance is the facility in which generated carriers move throughout the semiconductor material and the specificity of the hole- and electron- contacts that should extract only one of the carriers on each side of the Solar Cell [13]. A traditional solar cell made of Silicon(group IV) requires that foreign atoms that are either electron accepting(group III) or electron donating(group V) are infused into the active layer at different depth of the material to create selectivity through a p-n-junction, this process is called doping [14]. In Perovskite Solar Cells no doping is needed to create this selectivity but there is a natural barrier in the molecular structure of the compound that prevents immediate carrier recombination. Most commonly called Electron Transfer Material(ETM) and Hole Transport Material(HTM), the efficient extraction layers on the top and bottom of the solar cell active layer selectively extract each carrier type. When a conducting back contact is linked to each separate extraction material we get solar cell function [13]. If recombination occurs, the carrier-pair is joined and neutralised, sending out a photon with energy specific to the change in energy-level, which generally corresponds well to the band-gap. This phenomena is called Photo Luminescence(PL).

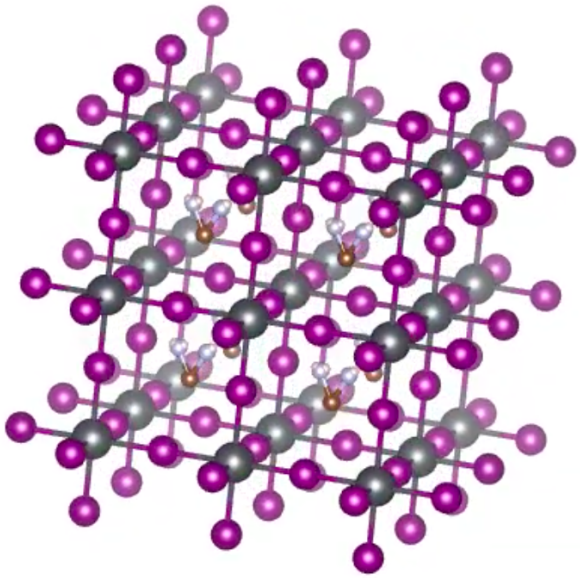

Figure 2.1: Vesta [15] model of $FAPbI_3$ 4x4 unit cells. Bond length accuracy not guaranteed. purple: Iodide atoms, black: Lead atoms, brown+blue/pink: FA cation. Notice the symmetry of the dodecahedral hole space in pure Pb composition.

2.1.2 Chemical composition of FA-Pb/Sn-I_3 Perovskite

Shown in Figure 2.1 is a model of the unit cell of cubic formamidinium lead iodide($FAPbI_3$ or FAPI), the model was created with Vesta [15]. Also called "FAPI", formamidinium-lead-iodide is a relatively new perovskite that has shown high efficiency but high instability. The cubic phase seen in the Vesta model is unstable and FAPI often adapts a hexagonal non-perovskite "yellow" structure at room temperature [16]. Constantinos et al. [17] have carried out a detailed study of the different crystal structures of pure FAPI and FASI($FASnI_3$) and how these differ from fully inorganic compounds, they observed that the transition of FASI to the α cubic phase occurred above 50 °C. It is interesting that both FAPI and FASI show thermodynamic instability where an increase in temperature leads to a more stable cubic phase. There are studies of how the unit cell and electronic structure varies with added Sn content for MA and Cs based perovskites [4] [7]. The band-gap can be significantly altered by only small adjustments in the crystal and the electronic structure changes during changes in structure such as deformation or strain [18]. The FA Cation in the dodecahedral space, in the middle of the lead iodide cubic lattice, has been proven to spin around at high frequency [19], it is not clear how symmetrical this spin is.

If regarding the creation of $FAPb/SnI_3$ as the mixing of two solid solutions FAPI and FASI there are two big risks when mixing two materials. The first is that the solutions will not mix and the second that they will go through phase separation. Effects such

as phase segregation and partial degradation are common phenomena. Mixing Sn into the lattice comes with another instability mechanism that is increased with increasing temperature.

2.1.3 Sn properties and problems

One of the main problems dealing with Sn-based perovskites is the high oxidation rate of Sn^{2+} to Sn^{4+} in environments with even small levels of oxygen. The Sn atom is slightly smaller than the Pb atom. Upon incorporation in FAPI perovskite, Sn is reported to have very low lattice perturbation in available literature [20]. Incorporation of Sn is assumed to happen as direct exchange with the (grey) Pb atoms seen in the model. Sn incorporation might help to stabilize the otherwise unstable 100% Pb FAPI cubic phase as nearest neighbour distances change, leading to a more thermodynamically stable phase. On the other hand, at certain compositions, Sn^{2+} ions might be more protected from oxidation in the strained lattice of FAPI. If the Sn^{2+} ions are oxidized to Sn^{4+} ions in solution however, the ions cannot incorporate into the lattice.

Methods

3.1 Fabrication Methods

3.1.1 Standard Perovskite Solar Cells

Fabrication of standard perovskite solar cell devices was done in normal stacking
SLG/Front contact/interface/ETM/Perovskite/HTM/Back contact
SLG/FTO/TiO_2-compact/TiO_2-mesoporous/Perovskite/Spiro/Au
The glass comes from previous fabrication with an FTO layer and is cut by diamond tip

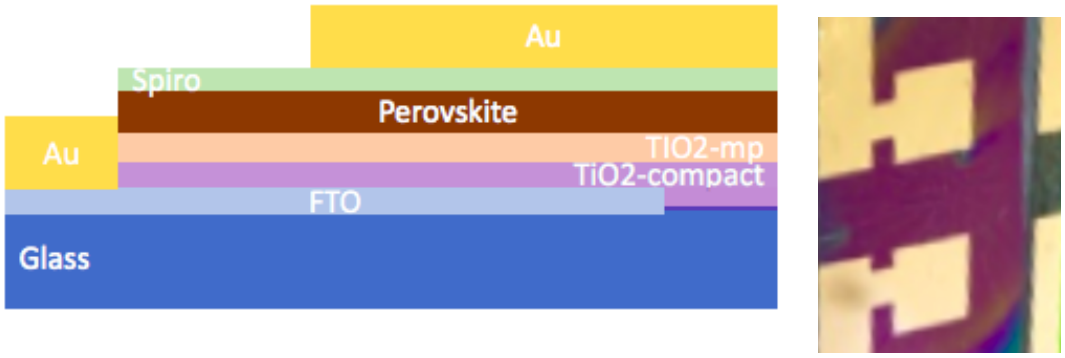

Figure 3.1: Design of standard PSC. Left: material stacking. Right: Au top contact design on a finished device

into marked samples. Each sample will contain two devices with an active area of 0.1582 cm^2 respectively. See figure 3.1 for device layout. FTO on the cathode side is removed by wet chemical etching with Zn powder and HCl to avoid short circuit formation and samples are cleaned by three respective steps of 20 min ultrasonic baths with Hellmanex 2%, Acetone and Ethanol. The compact TiO_2 is deposited by aerosol spray pyrolysis driven by 0.5 bar pressurized O_2 gas sprayed at substrates held at 450 °C with the FTO side edge protected. The precursor solution was made with Acetyl Acetone, Titanium

Diisopropoxide solved in IPA(75wt%) and Ethanol, and after drying the film should be around 100 nm thick giving a slightly purple colour. Between each step the substrates passed through UV-cleaning of approximately 15 min to make sure the interfaces were created as clean and connected as possible. The mesoporous TiO_2 paste includes many additives and is deposited through spin coating. To be able to deposit the dense paste is it diluted in ethanol at 150 mg/ml and after at least 12h stirring; 50 μl of solution is spin coated by 4000 rpm, 2000 rpm/s, 10 s, protecting the FTO edge with tape. The film is dried/sintered in a series of heating steps of 10 min 80 °C, 5 min 125 °C, 5 min 325 °C, 5 min 375 °C, 30 min 450 °C, cool down. Each heating step removes an additive or solvent and the sintering of the layer results in a complex mesoporous structure. The final film thickness achieved with this recipe should be 150-200nm. After being transferred to a N_2 glovebox the perovskite solution is deposited on top of the previous films by spin coating with CB antisolvent. After deposition, the samples are annealed at 100 °C for approximately 1h and left for cool down. Spiro-OMeTAD is solved in Chlorobenzene(CB) (92 mg/ml) and right before deposition dopants 50 mol% LiTFSI(1.8 M in Acetonitrile(ACN) and 330 mol% TBP are added. The spiro solution is deposited by spin coat recipe 50 μl], 4000 rpm, 2000 rpm/s, 20 s, immediately after perovskite layer annealing and cool down. Deposition of perovskite and HTM was done in N_2 glovebox, and afterwards the samples are placed in dry air storage for oxidation of the spiro. Before deposition of the electronic back contacts all films but the FTO doping layer on the SLG substrate are removed by scratching the FTO side edge of the sample. This created a surface for the electrode and avoided short circuits in the device, the edge is cleaned with Acetonitrile for adhesion. The contacts were deposited by thermal evaporation of 80 nm gold(Au), and defined through a shadow-mask. After Evaporation the samples are left in dry air in the dark before measurements on JV-setup. See Supplementing Information for a more detailed description of the fabrication process as well as a list of perovskite recipes used. The record cell used triple cation CsMaBrPbI3 solution in DMF/DMSO 4:1.

3.1.2 Sn-Pb-Mixed Perovskite Solutions

Tin-Lead mixture solutions were prepared by first making stock solutions of 1.2 M $FAPbI_3$ and 1.2 M $FASnI_3$ in DMF/DMSO 4:1. PbI_2, SnI_2 and FAI came in powder form, first a 1.4 M FAI in DMF/DMSO 4:1 was created during heating at 70 °C and this solution was then added to precise amounts of SnI_2 or PbI_2 together with some additional solvent(DMF/DMSO). The solutions were prepared by careful calculations of the exact molar proportions and several density measurements to ensure equimolarity of cation FA, and the inorganic B atom. Volumetric comparison was then used to create solutions of different composition with the mixed structure 1.2 M $FASn_xPb_{x-1}I_3$ in DMF/DMSO 4:1,

x ranging from 0% Sn to 100% Sn. A list of solutions created can be found in Supplementing information. Some $FASnI_3$ stock solutions had to be reduced with Sn-powder for approx. 1 week due to oxidation of the solutions even though preparation and storage was done in an N_2 Glovebox, and as time passed solutions needed longer reduction. The reduced $FASnI_3$ stock solution was filtered shortly before the mixed composition solution was created and deposited within 24 hours.

3.1.3 Thin film samples

Thin films of $FASn_xPb_{1-x}I_3$ with varied composition(x) on glass were extensively investigated during the project, only part of the study could fit in this report. Prior to deposition of Perovskite the glass samples of dimension approx. 1x2 cm^2 were cleaned with HellmanX, Acetone and Ethanol, followed by 15 minutes of UV cleaning shortly before transferred to a N_2 Glovebox. All perovskite was deposited using spin coating. In the process, parameters such as anti-solvent usage(Yes or No), spin coating program(Slow or Spin20), and whether samples were encapsulated(Yes or No), and how they were stored(Air or N_2) after deposition were varied and recorded. After deposition each standard thin sample was annealed on a hotplate at 150 °C for 30 minutes. The antisolvent used on some samples was Toluene, around 120 μl was dropped on the samples after 20 seconds of spin coating program. SpinSlow program was 2000 rpm, 200 rpm/s, 40 s. Spin20 program was step1 - 1 s, 2000 rpm, 1000 rpm/s, step 2 - 40 s, 6000 rpm, 2000 rpm/s, step 3 - 59 s, 6000 rpm, 6000 rpm/s. Encapsulation was done in N_2 Glovebox by using UV-hardened Epoxy. The epoxy was placed on a cover glass(same as sample) and placed together straight on the perovskite films and hardened under Ultraviolet(UV) light for 90 s. A table recording the exploratory study of all samples created and which parameters were varied can be found in the Supplementing Information, along with detailed definitions of protocols for those who wish to repeat the experiments. Figure 3.2 might give an overview of how the many parameters were varied during different fabrication steps.

3.1.4 New Methods in Perovskite Solar Cell fabrication

Once different perovskite mixtures were established on thin glass by spin coating the same experiment was repeated with other available deposition methods.

Inkjet Printing uses a highly controlled vacuum and microfluidics to create and drop very exact droplets onto a flat surface with calculated distance separation. That way perfect films with very high precision can be created. It is the same method used on paper in a home office Inkjet-printer today, and ideally this is a process that could be automated in a big room with no human contact, decreasing a majority of the negative

aspects of solutions handling [21]. The printer in our lab needed a considerable amount of configuration and optimization of drop size and step size before a film could be formed. This part of the project gave a good look into safety measures needed when working with lead containing organic strong solvents and a real sense to some of the drawbacks of perovskite manufacturing. Due to ventilation failure the experiment was cancelled and high health risks with air-born strong solvents containing Pb were documented by laboratory safety staff.

FIRA, Flash InfraRed Annealing, is a new method at LSPM developed by Postdoc Sandy Sanchez. The FIRA uses UV and infrared pulses to resonate with the FTO on the glass and creating quickly dissipating heat waves that anneal the liquid layer very quickly (2-20 s). FIRA annealing has been proven to generate larger grain size and a more homogeneous crystal [22]. The question was if annealing films with FIRA would generate a different result than normal spin coating and hot-plate annealing as to which different compositions of mixed tin-lead perovskite generate different results. First coating and FIRA was done on normal glass cleaned by Hellmanx, Ethanol and Acetone, followed by 15 min of UV-Ozone cleaning. The solutions are spin coated(SpinSlow) onto the sample and placed inside the FIRA for rapid annealing. A span of different composition films were fabricated, however due to rapid oxidation of the solution the samples were limited to 2,5 s and 3 s FIRA on 0%, 20%, 40%, 60%, 80% Tin in FASPI and 3cation solution(only 2,5 s). Even if the FIRA is located in a dry air glove-box the oxygen content in the atmosphere is significantly higher than in the N_2 glove-box and solutions with tin rapidly changed colour from yellow to blood-red. Another attempt at using FIRA for thin film mixed perovskite fabrication was still made, this time with conditions more similar to PSC fabrication. A TiO_2 blocking layer deposited by spray pyrolysis and UV-cleaned, this time on glass with FTO. One experiment with TiO_2 layer underneath the perovskite and one experiment with only UV-cleaned FTO glass was done. This time compositions of 0%, 20%, 40%, 50%, 60%, 80% and 100% Tin and triple cation solution(only 1.5 s) was done for FIRA time of 1.5 s and 2 s.

Encapsulation is a more and more frequent method to protect the PSCs from the environment [23], and encapsulation was done as described for thin film samples above.

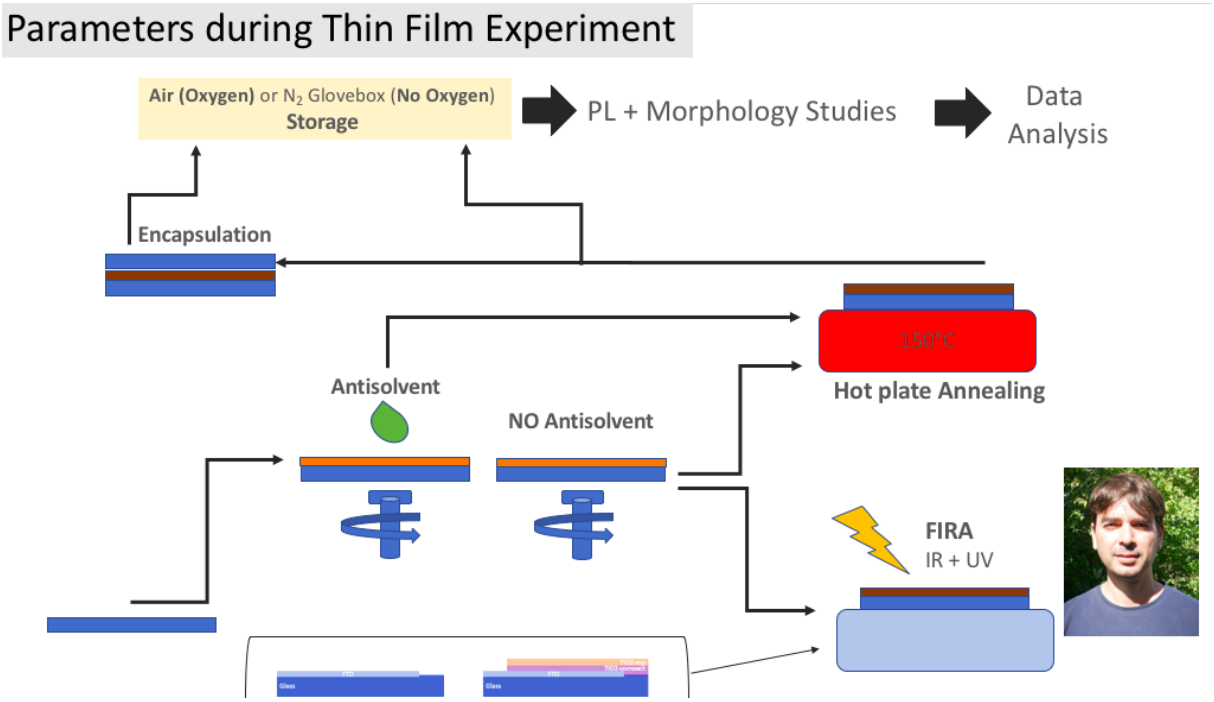

Figure 3.2: Layout overview of parameter variation during thin film experiments. At the bottom right a picture FIRA setup creator Sandy Sanchez [24] is displayed next to an illustration of the method.

3.1.5 Mixed Perovskite Devices

Sn-Pb-mixture sample devices were made with help from colleagues Hong Zhang and Jinno Hiroaki in two different stackings.
nip(normal stacking): SLG/ITO/SnO_2/Perovskite/Spiro/Au
Pin(inverted structure): SLG(thin)/ITO/PEDOT:PSS/Perovskite/PCBM(CB)/Au
The perovskite deposition was done in N_2 glove-box with 35 μl 3-step spin coating program Spin20(as defined above) and Toluene anti-solvent deposition after 20 seconds. After deposition of the back contacts the devices were encapsulated by methods described above, leaving the contacts exposed so JV measurements could be performed.

3.2 Characterization techniques

These methods for characterization are just some of the many measurements done on PSCs [25]. The methods explained here were used to make an exploratory study of the differences between samples made during the project.

A **Current Density(J)- Voltage(V) measurement(JV)** is the most common way to evaluate how well a PSC can be used as an electricity generating device [25]. A sun simulation lamp, most commonly using a spectra meant to simulate sunlight called AM

1.5 G source, shines upon the sample cell active area. During this excitation a load is first put on a silicon reference sample and then on the actual sample, plotting the Current Density while scanning the Voltage. Changing scan rate and step size affect the results so JV-measurements might not give a definite answer about efficiency for real application, but are used for getting a general view of the PV properties [25]. For the solar cells produced in this report the measurements were done in ambient conditions but with a flow of dry air to prevent excessive degradation.

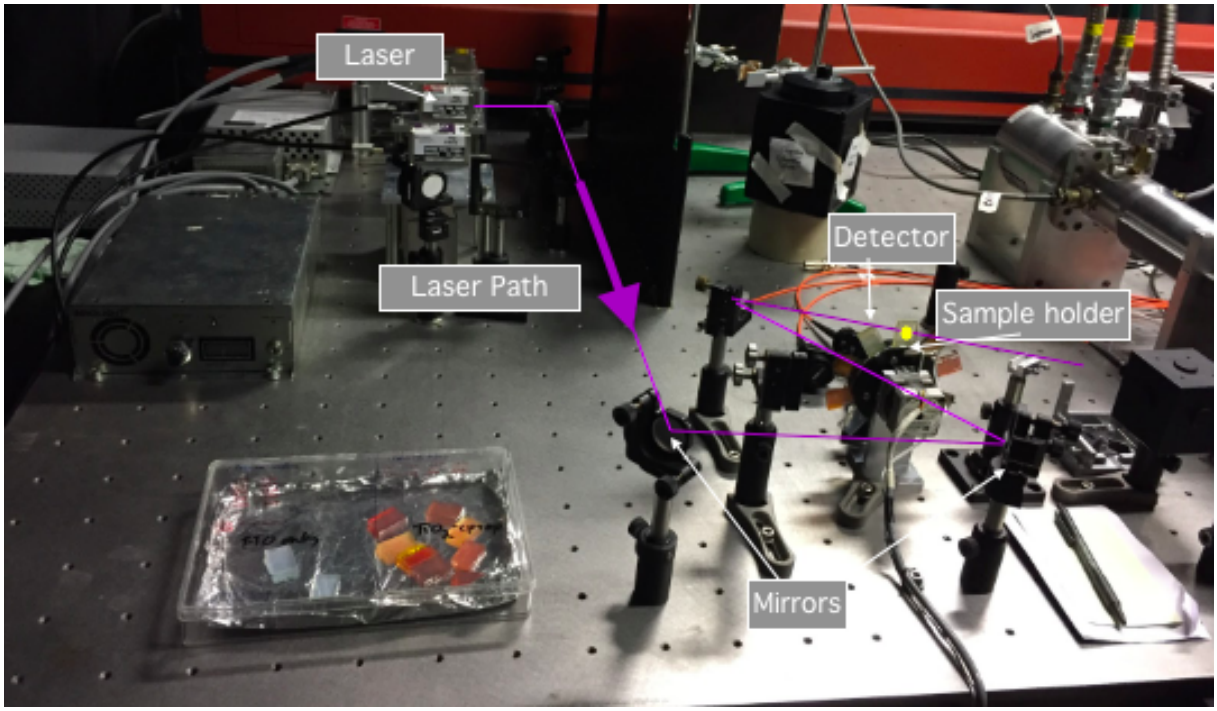

Figure 3.3: SS-Photo Luminescence measurement setup. Lasers, mirrors, sample holder and detector are strategically placed on an optical table. The optical table ensures stable mounting and suppresses vibrations from other machines in the building and from for example the rotating sample-holder to make sure the laser stays perfectly aligned.

Steady State Photo Luminescence(SS-PL) measurements are simple in principle; a sample is illuminated, light with the right energies will be absorbed, and eventually, as the crystal relaxes back from excitation, light is emitted from the sample in all directions. If a sample is illuminated by a laser from one side and a detector is set to detect only light that has been emitted from the sample (excluding reflections and transmittance from the laser) a clear signal from the Photo Luminescence of the sample can be achieved. In practise this requires a more complicated setup of well aligned mirrors and lasers. Shown in figure 3.3 is an image of the SS-PL setup with different key components pointed out. The PL arises from recombination of carrier pairs and in semiconductor the maximum

intensity wavelength, λ, can be related to the band-gap(E) of the material via planks constant, $\hbar$, by E = $\hbar$*v /λ, Einstein's equation. The measurements were done using an Obis laser 660 nm, a set up of mirrors and an Andor(iDus) Solis Spectrometer with an integrated low-pass filter at 700 nm (only photons above 700 nm should give signals). The laser power varied from 1 mW to 50 mW and mostly 660 nm excitation wavelength(blue) was used. The integration time was one second(Counts = Background corrected/s) and the total measurement time varied between 1-5 s for accuracy while the spectrometer was not saturated(at approx. $4 * 10^5$ counts per measurement).

X-ray Diffraction (XRD) from a sample can portrait at what angles from the sample you have constructive interference of X-rays via Bragg's law, giving information about long range ordering in the crystal bulk. Due to certain lattice distances and therefore specific spectra for certain phases and atoms in the material a fingerprint method can be used to probe the composition in the sample. XRD results are not always easy to interpret. Large databases for comparison are helpful to try to pinpoint the exact composition, thanks to use and data collection, frequently used materials can be identified. In this work XRD was used to relate PL peaks to certain XRD peaks and to compare XRD for different compositions. The EMPYREAN apparatus uses a Beryllium Laser and collection angles were varied from 10°-70° using a silicon strip detector.

A **Scanning Electron Microscopy (SEM)** image may achieve higher resolution than images by optical microscopy because of shorter wavelength of electrons compared to visible light. The sample is exposed to an electron beam in Vacuum and electrons are collected as they are emitted back from the surface. This gives information about the surface structure and can construct a 3D like image. Corners and edges of for example a crystal are highly visible since they posses a higher Surface to Volume ratio and can emit more electrons back into the Vacuum chamber [26].

Confocal Microscopy(CM) uses optics and do not need Vacuum to operate since light passes through air without considerable broadening, therefore this microscopy method is easy to use and can give quick information about the morphology of thin films. The confocal microscope used in this work could achieve a magnification of x10 or x50 and could operate in bright field or reflective mode. In bright field the light is collected on the back side of the sample, while in reflective mode only light that has reflected of the surface detected.

3.3 Experimental Setup and Data Analysis

PL-Stability investigation.
One of the main experiments in investigating differences between different FAPSI compositions consisted of investigating the film quality and degradation over time on thin film samples, this was done by SS-PL. Most samples degraded quickly so priority was given to attempting clear PL spectra peaks at around 1000 counts/s intensity, this was done by varying the laser intensity. For all samples at least 3 PL measurements were done at different dates, between measurements most samples were kept in N_2 glovebox(Protocol1). Two batches of samples were stored in air to produce more rapid degeneration(Protocol2). SEM images of some samples were taken to see film morphology on a smaller scale. Each sample had an individual tracking and at the end of the project factors were compared to see how trends when varying the composition changed with methods. Variables documented apart from Composition of Sn were deposition method, encapsulation, solution batch, anti-solvent/no anti-solvent and whether samples were stored in air for degradation or N_2-glovebox for longer storage. See Supplementing Information for detailed tracking of PL measurements. All FIRA samples were also tested for stability with PL and XRD. XRD measurements were done to identify different phases that responded to PL peaks on the different films. Samples that showed interesting PL peaks were selected for XRD1, these peaks were then used to try to identify some degraded or stable phases resulting from long time storage of the mixture-samples. After XRD, the SS-PL measurements on these samples were repeated. Following, for XRD2, new fresh samples with and without antisolvent were created and put in the XRD within 1 hour of fabrication to examine the peaks at the beginning of sample degeneration. These XRD were used for comparison between alloy concentration and spectra. Finally, for XRD3, fresh samples were done by FIRA to see if there might be any difference in the result. After XRD2 and XRD3 the newly created samples were investigated by SS-PL to search for further phase-matching and see stability over time.

Data Analysis.
The data from PL and XRD was analyzed with computer scripts *Thot Analysis* at the end of the project, in collaboration with Brian Carlsen at LSPM EPFL [27]. *Thot Analysis* is a new software created by Brian that does bottom up analysis of data so that comparisons for correlations can be seen more broadly and clearly. Since the software is recently developed the collaboration included problem solving and investigation of which data-parameters could be transferred through the levels of analysis, leading to significantly more work than expected. See figure 3.4 for an example of the data extraction from a PL

measurement.

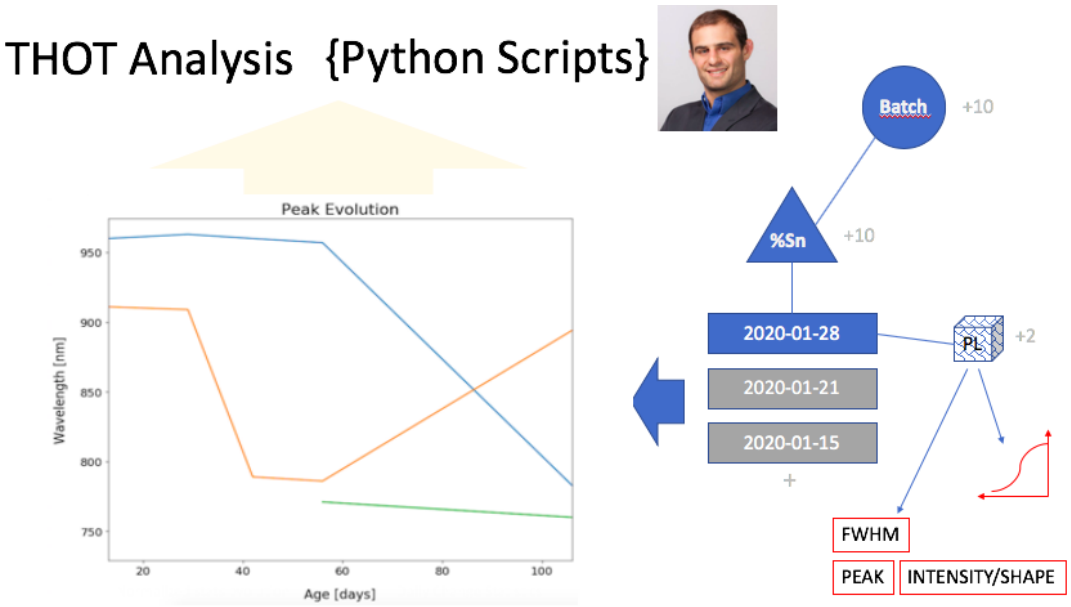

Figure 3.4: Image explaining a specific analysis sequence of Thot and some parameters extracted at each level. Featured a picture of Thot creator Brian Carlsen [28].

Spectras of measurements were visualized using scripts in Jupyter notebook, Origin and Matlab. Device data as seen in the report are plotted using seaburn boxplot in jupyter notebook. Graphs of JV scans are taken from Macros output of the local analysis program in the JV-setup. Plots from Thot analysis are visualized using Matplotlib. Visualizations of crystal-lattices were done in Vesta. The report is written in Overleaf and some images are modified using Microsoft PowerPoint and Sketchbook.

Results

4.1 Standard Solar Cells

The record devices for each batch had PCE of 16.01%, 16.84%, 19.51%, 16.6% and 18.47% respectively. Other record parameters as batch fabrication was repeated varied as following; 19.53 mA/cm^2, 22.96 mA/cm^2, 22.15 mA/cm^2, 22.65 mA/cm^2 and 23.62 mA/cm^2 Jsc, 1.07 V, 1.08 V, 1.32 V, 1.04 V and 1.07 V for Voc and 0.701, 0.687, 0.777, 0.71 and 0.758 for FF.

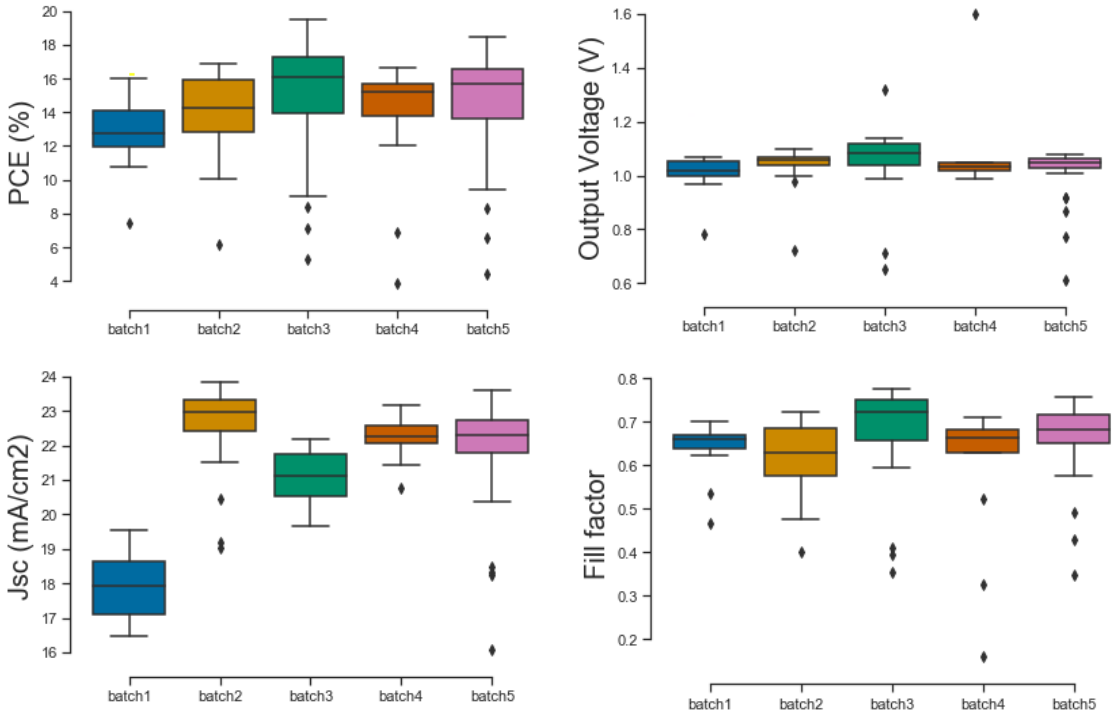

Figure 4.1: Photovoltaic performance of fabricated Standard Perovskite Solar Cell Devices and how developed during repetition of the recipe.

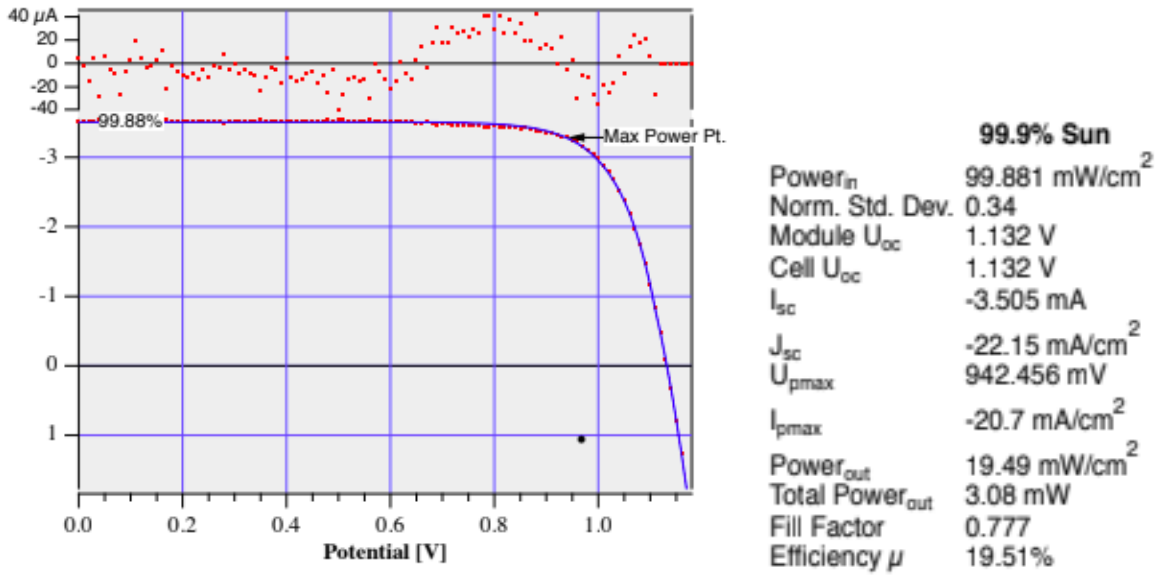

Figure 4.2: JV measurement for Record Standard device, PCE 19.51%.

4.2 Sn-Pb-Mixtures Study

For an objective and comprehensive overview results for this part of the project would need to be placed in detailed 3D plots, or a long report including many samples would need to be disclosed. The short summary that is this report would not be enough to make the complete analysis comprehensive to the reader, especially without extensive data analysis. Such analysis could unfortunately not fit within the time-frame of the project, but great efforts have been taken to select a few examples that can give a sense of what was done. This result section is an attempt to show some observational trends in each section were changes were investigated. Further data can be found in Supplementing Information or by reaching out to the author.

4.2.1 Visual Effects

Visual effects were documented during the project by mobile-phone photographs. An example of resulting films are seen in the photographs of Figure 4.3. Recently fabricated films by anti-solvent method spin coating and hot plate annealing with composition of Sn increasing from left to right (top image) are compared to samples with after 1 month in a laboratory drawer (bottom image). In Figure 4.4 are Images of samples coming out of the first batch done by FIRA on cut optical glass-slides. The second image is the films after 1 months time, showing much less change than the samples prepared by anti-solvent method.

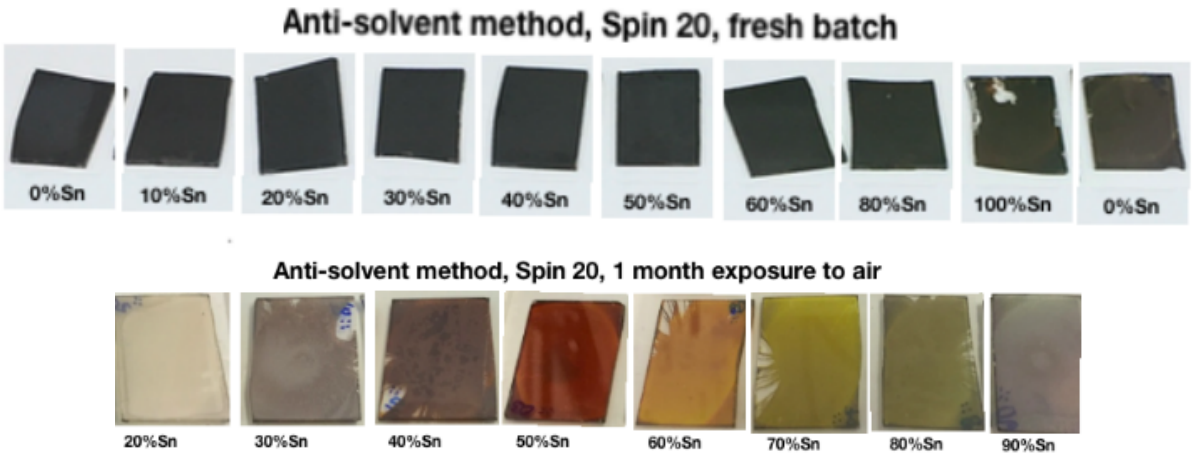

Figure 4.3: A comparison of newly fabricated films created by anti-solvent method (top) and films created by the same method and exposed to air for 1 month (bottom).

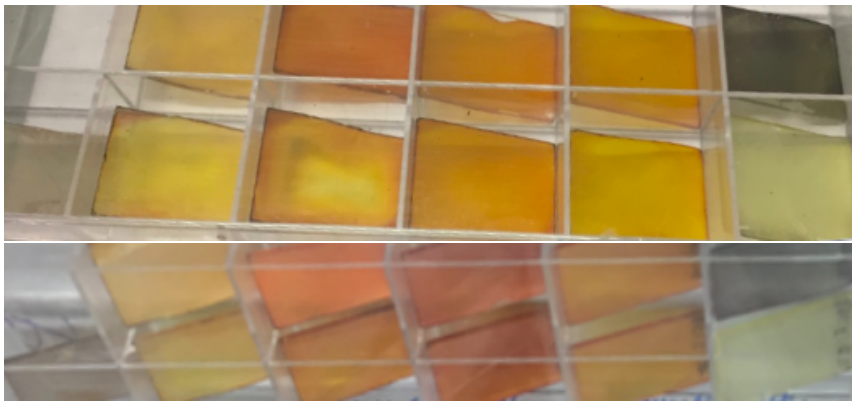

Figure 4.4: Image 1: FIRA batch 1 just after fabrication. Image 2: FIRA batch 1 at end of project after storage. top row is 2.5 s by FIRA exposure and bottom row is 3 s by FIRA. Compositions from left to right: triple cation recipe(only 2.5 s, bottom row), 80% Sn FAPSI, 60% Sn FAPSI, 40% Sn FAPSI, 20% Sn FAPSI, 0% Sn FAPI.

4.2.2 Morphology

How the morphology was affected by varying Sn ratios was investigated by CM(bright field and reflective) and SEM. Once again a big study was done and more analysis is needed to present concrete evidence of differences, but the trends observed were prominent and presented here are some examples. First, in Figure 4.5, samples done by FIRA with pure compositions in a closer look with CM are presented. In Figure 4.6 more interesting morphology, varied compositions, are shown for the same batch with variation only in the Sn ratio in the mixed perovskite film. The samples were made by No-anti-solvent method, images taken with CM at the same magnification(x50) as Figure 4.5. The darker structures, cubic phase perovskite, was more 3D shaped than the more yellow flat layer

underneath.

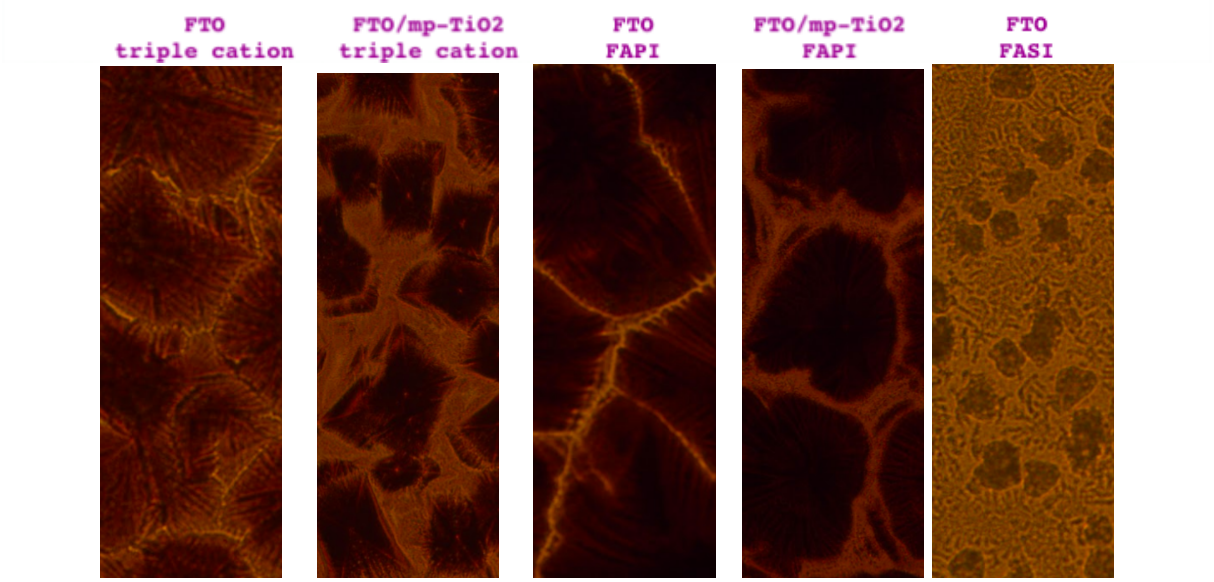

Figure 4.5: A Confocal study of the morphology of pure compositions $FAPbI_3$ and $FASnI_3$ by FIRA(standard 2 s).Approximate real space width of the images: 60 μm.

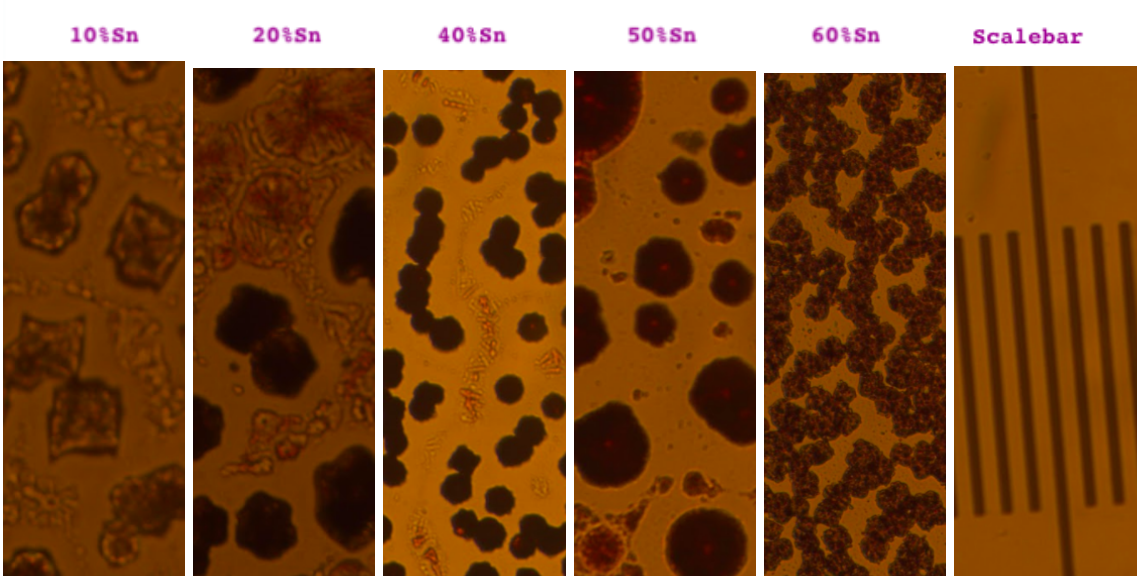

Figure 4.6: A Confocal study at Mx50 after 3 months storage in N_2 Glovebox. Films were fabricated by No-Anti-solvent method. Approximate width of the images is 60 μm. Far right: an image of the scale bar in same magnification(x50), each step representing 0.001 cm.

4.2.3 Photoluminescence spectra over time and band-gaps

In Figure 4.7 is an example of the degradation of a thin film (No-anti-solvent method 60% Sn FAPSI in air degradation(protocol Air)) as seen in SS-PL.

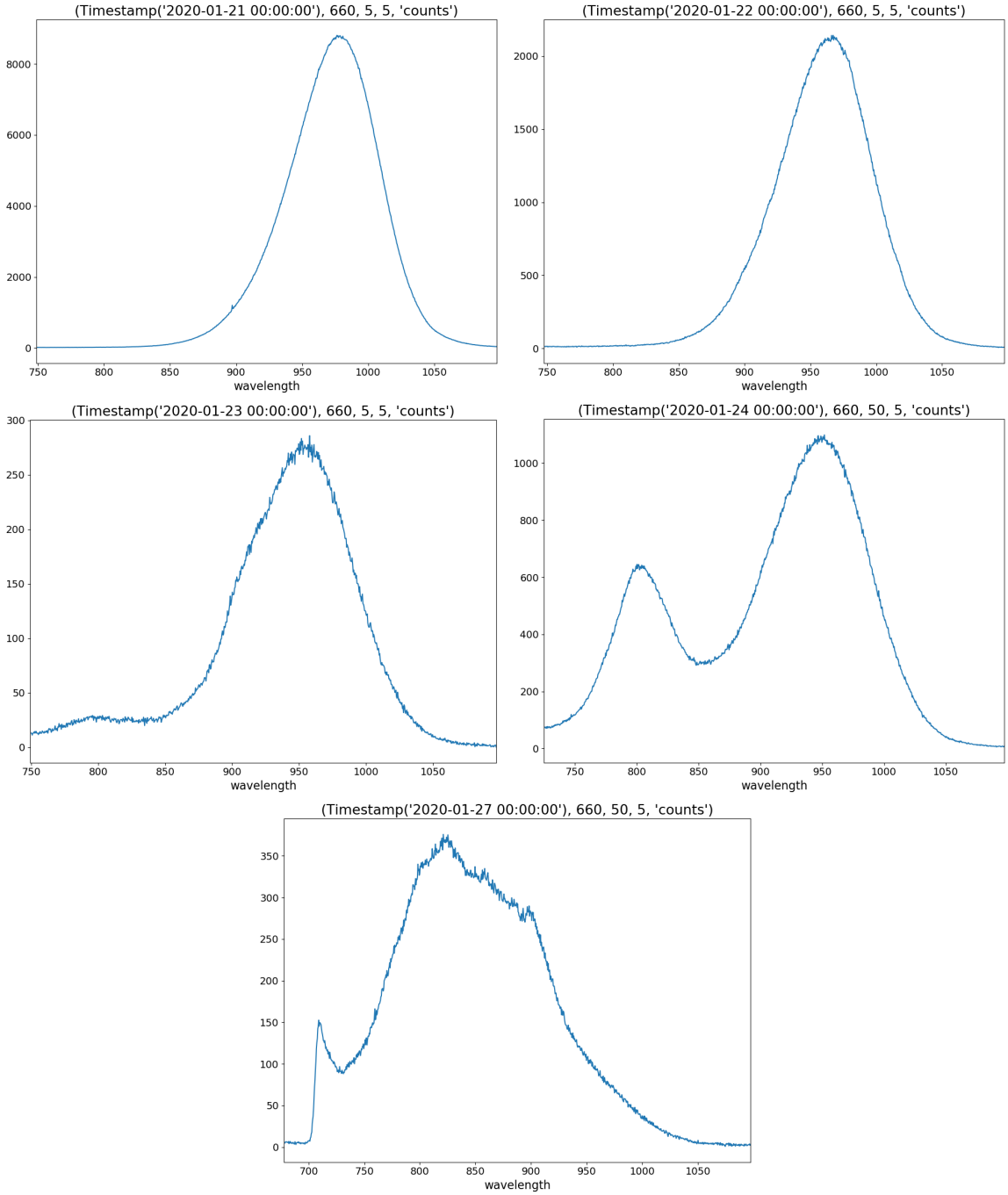

Figure 4.7: 60% Sn No-antisolvent method sample fresh batch, degraded with protocol 2 in air for one week. The feature on the left in the last image is leakage from the 660 nm laser since the low-pass-filter was not fully efficient

At one instant the stability under laser exposure was measured on a 40% Sn sample (Batch7AirAntisolvent40% Sn), the laser was kept on and measurements were done up until 5 minutes exposure, then measurement 5 and 15 minutes after turning the laser off

was done to observe recovery. In Figure 4.8 the PL spectra at a few instances are seen. As can be seen the PL spectra undergoes changes that are partly restored after some rest in the dark.

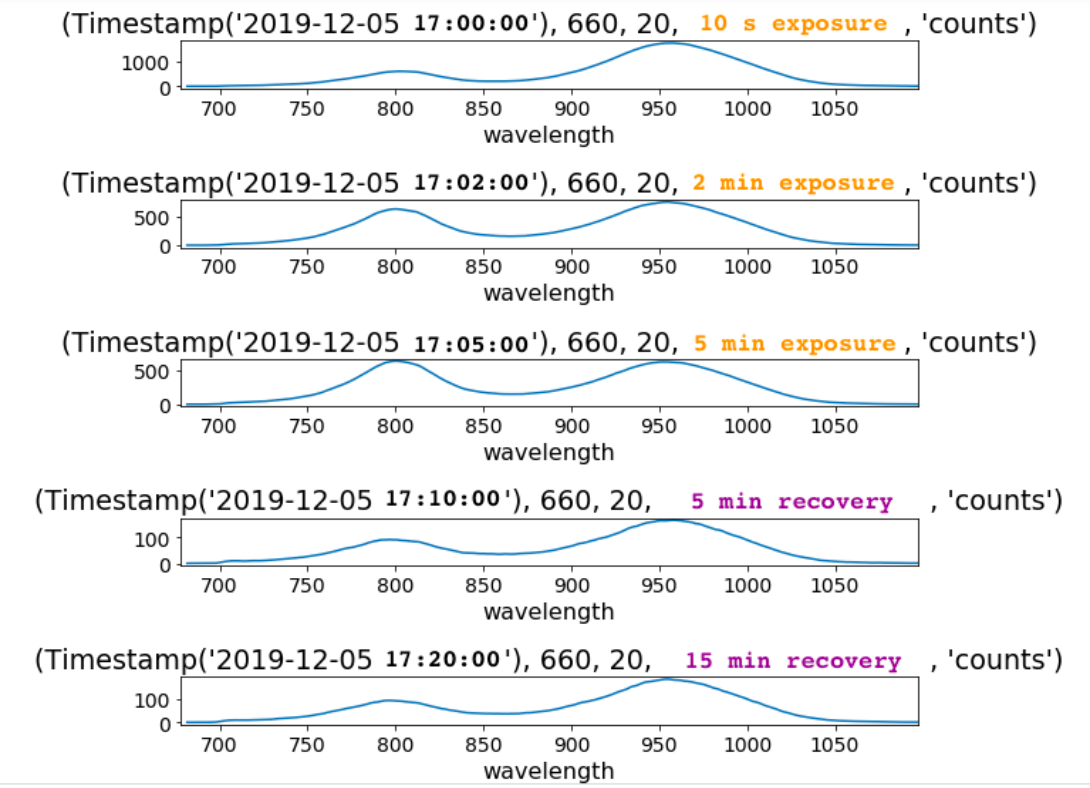

Figure 4.8: Effect of prolonged light exposure on 40% Sn sample done by anti-solvent method, followed by resting the sample for 15 minutes. Excitation wavelength 660 nm, laser power 20 mW, 5 seconds integration time. Y axis is background corrected counts/second.

PL measurements and the band-gap of the perovskite films can be approximately related by Einstein's equation(see methods section). In Table 4.1 is an approximation of band-gaps taken from the first PL measurement of samples with different composition, these values are slightly higher than literature for the same compositions [29] [30]

Table 4.1: Observations of PL peaks at first measurements, the values showing the *median*, which in most cases was also the most common value. Note that the purpose of this table is to give a more numerical overview and that no statistical tests were done. Compositions that did not give any clear peak positions were removed. Band gaps are calculated by Einstein's equation ($E = \hbar * c/\lambda$).

Recipe	**3cat**	**0%**	**15%**	**20%**	**25%**	**30%**	**40%**	**45%**	**50%**	**60%**	**70%**	**98%**	**100%**
PL peak (nm)	770	818	920	917-960	930	940	960	965	970	970	964	934	894-918
Corresponding bandgap (eV)	1.61	1.51	1.34	1.29-1.35	1.33	1.32	1.29	1.28	1.27	1.27	1.28	1.32	1.37

The band-gap taken out from PL spectra of triple cation samples is approximated to 1.61 eV (PL peak 770 nm). Just as the colours seen in the visual images the band-gap show more changes in the outer ranges of compositions. Between 40-70% Sn in FAPSI the band gap stays below 1.3 eV with a minima at 50-60% Sn.

In Figure 4.10 and Figure 4.9 the wavelength at peak position is taken from the SS-PL measurements of all FAPSI films and a 3D plots are constructed. Composition in % Sn is plotted against wavelenght position of the peaks. Measurements from each sample and experiment during the entire project are included.

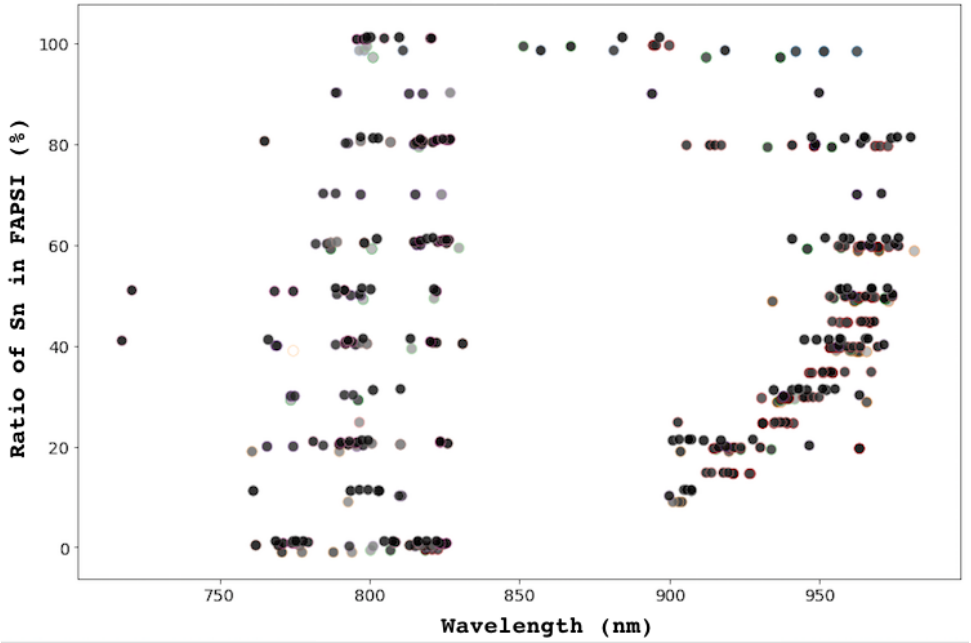

Figure 4.9: Distribution of PL spectra sorted with composition(%) of Sn in $FASnPbI_3$ and wavelength for the max peak position at measurement. The gray-scale colours of the dots represent the age of the sample, with darker colours being older samples. Edge colours represent different batches.

In the figures it becomes clear that most Sn containing films showcase a PL peak around 800 nm at sometime during measurements. Noticeable is that non of the 0% Sn films showcase a peak at 800 nm, yet the 800 nm peak is more centered and narrow in lower concentration of Sn. There seem to be another phase separating out with high Sn content around 850 nm, seen at some measurements at lower Sn but very prominent at 80%Sn. There is also a peak around 900 nm that is slightly shifting to the left with higher Sn concentration, but it is weaker than the other peaks mentioned. The band-gap curve as seen in Table 4.1 is reflected in the curvature to the right in the figures, it is also noticeable how the spread in wavelength changes with composition. There seems to be a wider spread in wavelength (and thereby band-gap) at higher Sn ratios. A part of this

spread could be because of the shoulder features such as seen in Figure 4.7. The 100% Sn films seem to be highly unstable with few accumulation of measurements at other places than PL 800 nm and 850 nm.

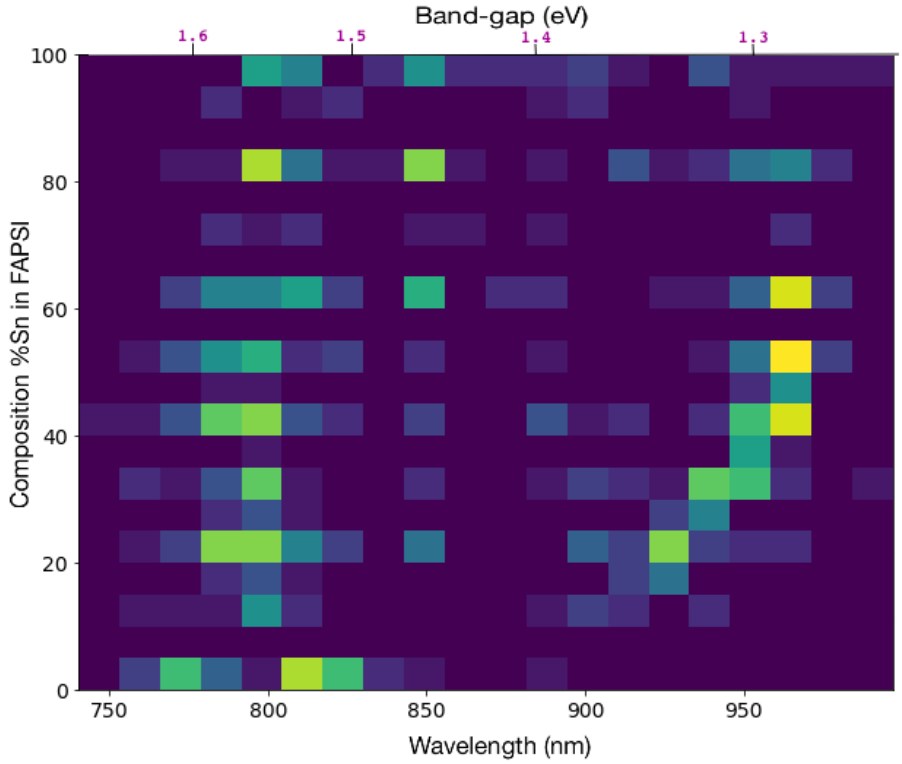

Figure 4.10: Peak density PL, all measurements. Areas with higher density of measurement points are represented by lighter pixels. The band-gap axis on top of the graph is an approximation by Einstein's equation.

4.2.4 X-ray Diffraction

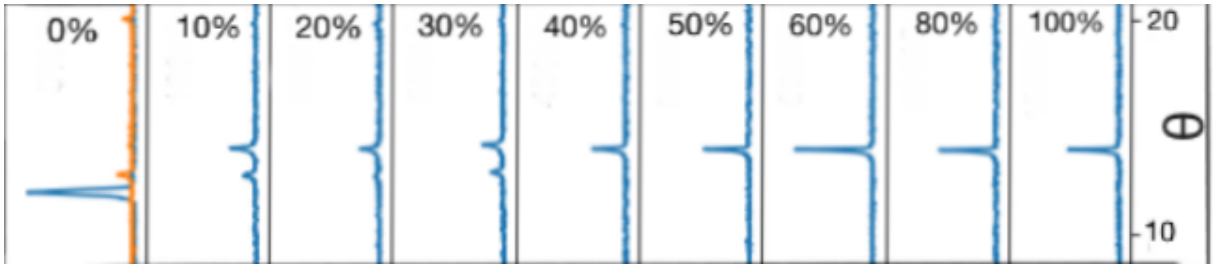

Figure 4.11: A look at the 14 θ peak of an ant-solvent batch

For XRD2(fresh batches anti-solvent and no-anti-solvent) and XRD3(fresh FIRA) peaks were compared by making stacked plots and it became clear that different substrates once again showed differences as well as different compositions. Peaks changed the most during

composition variation in XRD2, in XRD3 they stayed more constant. The 14 θ, 24.5 θ and 28.31 θ peaks changed significantly. and peaks changed the most in Anti-solvent samples. The time span for this project did not give for identifying the phases and components of the samples. Comparison of peaks from XRD1 with PL spectra led to "guesses" of which XRD peaks could correspond to certain PL peaks but are not presented in this report.

4.2.5 Performance of Tin-Lead Mixed Perovskite Devices

Batch 1 with nip-structure did not have great results, with PC efficiencies below 0.5%. Result Voc for the record cell with 60% Sn was 0.34 V, the Jsc was 2.55 mA/cm^2, the FF 0.499 and the PCE 0.43%. The efficiency was measured several weeks after completion of the device but the result was still not encouraging for nip-stacking of Sn/Pb-mixture PSCs.

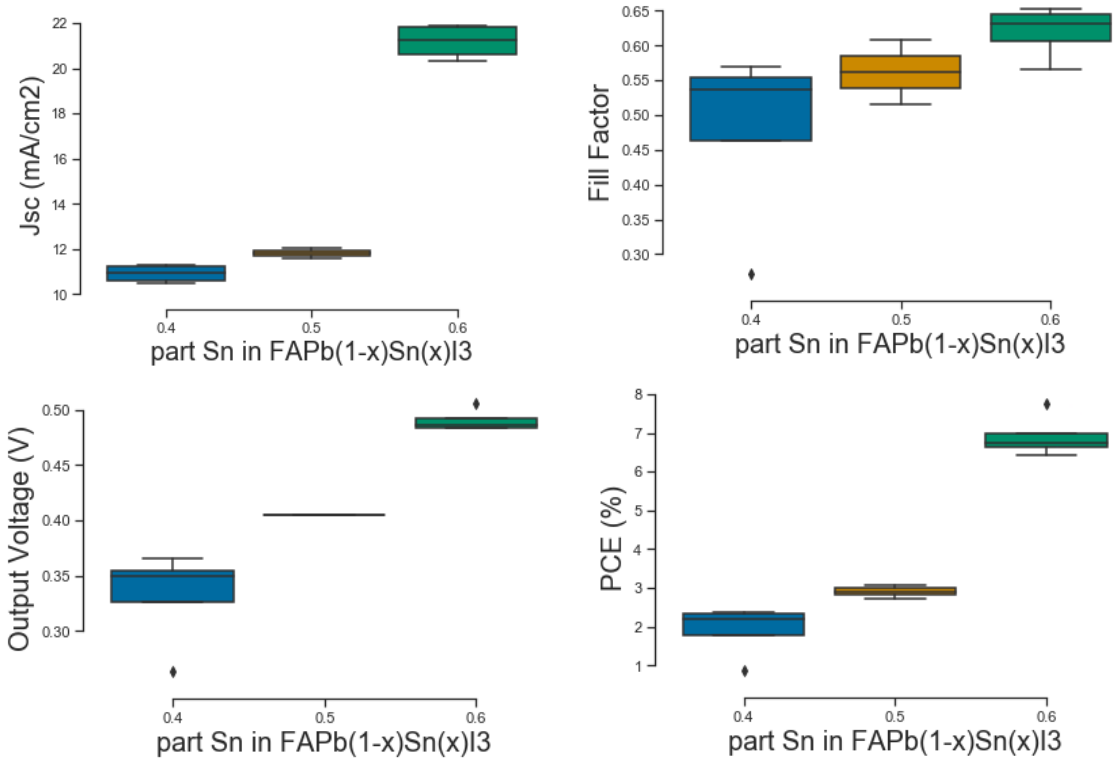

Figure 4.12: JV measurements of $FASn_xPb_{1-x}I_3$-perovskite devices with pin inverted structure, x axis label indicating the value of x.

The mixed PSC with pin-stacking did significantly better as can be seen in Figure 4.12. A mistake was made when samples went into evaporation due to problems with the machine, and labels were lost, so the identification was done by comparing the narrow span of Voc with previous results. With a record PCE of 7.76% the 60% Sn device stood out, having a

high Jsc of 21.9 mA/cm^2, a Voc of 0.653 V and FF of 0.506. During the experiment it was noted that the morphology of the films looked very nice, especially compared to another recipe that was tried by colleagues. This indicates that the 40%-60% Sn compositions worked quite well as indicated by previous PL study and a good fit with Toluene anti-solvent.

4.2.6 Discussion

It became clear that different levels of Sn concentration show different morphology, PL, XRD and PV performance than others. The results indicate that exchanging Pb for Sn is a tool for changing the characteristics of perovskite films. The results show changes in bandgap, stability, morphology and phase separation. From visual investigation it seems as if the FIRA-method creates a more stable morphology that does not change as much over time, whereas the anti-solvent-method creates high quality films that are more unstable and degrade more unpredictably. Most importantly films behaved differently depending on the composition, were some compositions showed more suitable for PSC fabrication than others. Some similarities between samples were seen in PL-investigation, where features seen in PL could be related to the presence of different phases at different life-stages of the films. The mechanism of degradation seem to involve phase separation and the creation of a phase that gives PL intensity around 800 nm. This peak seems to correspond to the 14 θ peak in XRD. From differences when comparing all of the measurements together in Figure 4.9 it is probable that the compound giving rise to the 14 θ XRD peak and the 800 nm PL peak contains Sn.

The experiment of Figure 4.8 gives indication of light induced phase separation in the 40% Sn FASPI sample, meaning that as the film is exposed to radiation part of the phase giving rise to the 960 nm PL peak separates into the phase giving rise to the peak at 800 nm. Questions arise weather the phase that give rise to the 800 nm peak could help stabilizing the film or if it is an unwanted phase arising from breakdown of the perovskite. The recovery upon rest for only 15 minutes indicate that the generation of carriers might create some instabilities within the material.

A sharp rise in efficiency was seen between the 50% and 60% Sn cells. This seems to be mainly because of highly increased Jsc. Safe to say the Sn addition increased the Short Circuit Current Density of the perovskite, and hopefully, by improving the device parameters to increase FF and Voc, devices with even higher PCE can be achieved.

Discussion

5.1 Standard Solar Cells

The development in photovoltaic properties of the standard PSC with triple cation depended greatly on the quality of fabrication. Over 5 different batches an improvement was first seen but evened out in the end. A personal goal for this part of the project was to achieve over 20% PCE on the record cell, and 19.51% is close. Once the skill of executing the fabrication recipe was developed the median of the parameters for the last 3 batches did not vary significantly. In continued experiments more controlled fabrication steps and better cleaning before deposition processes might improve weaknesses in spiro connection and the quality of surface before perovskite deposition. Another improvement would be using density measurements on solutions when mixing precursors to get more precise compositions.

The parameter that varied the most between batches was the Jsc, especially when increasing from 19.53 mA/cm^2 on the record cell of batch1 to 22.96 mA/cm^2 on the second batch record cell. There was even one cell in batch2 with Jsc of 23.85 mA/cm^2. The Voc of the devices was quite stable since the device layout and program didn't change, however the record cell from batch 3 and one outlier in batch 4 stood out significantly. The outlier device in batch 4 had Voc of stunning 1.6 V, but the FF was below 0.7 and Jsc was 21.75 mA/cm^2, leading to a PCE of only 15.52%. The Fill Factor varied as well, it significantly went up for the record batch nbr3.

5.2 Sn-Pb-mixtures Study

5.2.1 Visual Effects

The differences in visual effects were considerable. Newly prepared films all had similar visual cues; samples had black, smooth and shiny films and no differences between compositions could be documented. After only short exposure to air the colour changed, the resulting colour depended on the amount of Sn present in the perovskite as seen in the bottom image of Figure 4.3. Anti-solvent prepared samples changed more than samples prepared by other methods. Middle range compositions seem more stable than the outer-range composition samples. The 40% Sn seem to have maintained most stability. The changes on FIRA samples seem less prominent than changes on anti-solvent fabricated samples and films by FIRA seem to have reached a more stable state at once. It was also shown that the substrate will impact the visual effects and structure of the thin films, even regarding what compositions show more changes.

5.2.2 Morphology

It becomes clear that different pure compositions yield different symmetries and shapes of grains. Noticeable is the pure FASI phase that showed almost no stable cubic phase. This illustrates the different instability mechanisms present in different pure compositions, and might help to visualize how a solid mixture of the compositions may look. Here its were too small to analyze by x50 magnification. is also clear just as reported in [31], that FIRA result in bigger grains than other methods like No-anti-solvent method shown in Figure 4.6 or anti-solvent method were grains are very small.

Here it is clear that grains show different sizes, shapes and also different phase ratios. Interestingly the grain size seemed to follow the trends reported in band-gap [30], not consistently increasing or decreasing but showing more of a wave-tendency with increases and decreases periodically. The 40%Sn and 60%Sn showed most consistency in connectivity between grains (morphology) and maintained visual appearance.

5.2.3 Photoluminescence spectra over time and band-gaps

There was a logical coincidence between connection between grains as seen in CM and the intensity and stability of PL spectra, and 40% and 60% Sn showed most consistency in these both factors. As the sample degrades the PL ”weight” is shifted towards a peak with max intensity at around 800 nm. This was a common trend in most mixed samples. Other trends seen clearly was a decrease of intensity and the appearance of shoulder features such as the one seen in measurement 3 in Figure 4.7.

Notice in Figure 4.8 how the 800 nm peak gradually increases as the film is exposed to the laser and then decreases as the film is left in the dark. The original shape at 10 s exposure is almost completely recovered after 15 min recovery, yet the overall PL-intensity has decreased.

Project Work 4. International Data-base collection

A larger effort to categorize the perovskite research globally is taking place. Our work included reading 200 articles about perovskite each and filling in excels that will be used by researchers at HZB to create a big database. This part was done at the very end of the project(December until end of April) and was a good complement to report writing, finalising in a very good overview of the field.

As articles about Perovskite Solar Cells are published in abundance it is understandable that many research efforts seem to go in the same direction and that many projects might be misguided. I gladly noted that in at least the 200 articles I read there was no experiment done like mine where the stabilization of FAPI could be related to changes in Sn composition only, even if some articles came close to the subject and could serve as inspiration and sources for the report. Further conclusions about this matter can only be drawn after publication of the entire project.

After reading 200 articles a great overview of the field was obtained and my hopes are to be the main author of publications some day. I have found some guidelines on structure, content, methods writing and how to give clear indications about the results by reducing text. Hopefully this work might lead to more success in future publications.

Conclusions

Personal knowledge an skill in PSC fabrication has been greatly improved during this work. High efficiency cells came close to the target at 19.5% PCE by developing the method of fabrication through repetition and by confirming the importance of deposition skill and interface connection for performance. This knowledge and practical skill was then applied to investigation and high quality of following work could be ensured. In general the aims in Sn/Pb exchange investigation could be fulfilled by giving an overview of some changes seen in morphology, stability and phases present for different compositions of $FAPb_{(1-x)}Sn_xI_3$, however data collection was extensive and the time ran out before full data-analysis. Following is an overview of some conclusions that were drawn during the project.

7.1 From experimental data

- Making PSC is a complex matter that is highly dependent on fabrication skill. Still in this work cells with over 18% PCE showed to be reproducible with triple cation recipe.

- Some compositions of Sn/Pb mixtures are clearly more stable and efficient than others. There is also a big difference in morphology as seen by CM. These results might depend on the bond length and strain compensation within the unit cell of the perovskite, or certain compositions better blocking the oxidation process of Sn^{2+} to Sn^{4+}. Just in 2020 an article was published in Nature describing the strain compensation needed for stable FAPI, but in this case it was done by growing the perovskite layer on a mismatched substrate [32].

- 40%-60% Sn seems to be the best interval for low bandgap (1.2-1.3 eV) cells with high absorption in the visible and IR spectrum. The 60% Sn cell with pin-stacking

had the so far highest result with over 7% PCE and high Jsc, while other parameters show great space for improvement.

- Encapsulation of FA(Sn/Pb)I_3 films gives a clear advantage to maintaining stability and more long term absorption properties, indicating that exposure to air is more detrimental than exposure to light.

- FIRA needs to be done in an oxygen free environment for Sn/Pb mixtures, with the current setup the oxygen levels in the glove-box were too high. Apart from the oxidation the method seems to be working well. After optimization 3 s pulse of 12000 W and waiting 20 s was the best recipe.

- A Phase that takes some part in degradation of mixed Sn/Pb perovskite films has been identified at 800 nm PL and 14 θ, it seems to contain some amount of Sn. The exact composition and structure of the phase could not be determined but experiments that show light induced phase separation give clues to that it takes part in the stabilization mechanisms of the carrier generating structures.

7.2 Observations

- Because of the high instability of 100%Pb FAPI and the development in stability while adding only certain % of Sn to the crystal matrix, speculations about the symmetry of spin of the FA-cation arise. Might this be from a high strain build up? The question is weather this strain arises from the increased size of the FA-cation or it's unsymmetrical electronic wave-function/spin.

- The general toxicity of solvents have been noted during the inkjet-esperiments in this project, and it is arguable what effect aggressive anti-solvents have if the intent is to create highly crystalline materials. It is clear from visual studies that grain sizes by anti-solvent method are very small and that the samples show big changes over time. There is other work arguing for the removal of anti-solvents from the fabrication processes and finding other methods [31].

- The $FAPbI_3$ perovskite showed a faster crystallization than triple cation perovskite, leading to believe the process might be favorable in comparison for industrial application.

7.3 Future prospects

- I greatly encourage to do similar experiments also looking at the density of the solutions to see if the result is consistent. Concentration variations would lead to different active-layer thicknesses that could impact the stability and PV performance.

- Further investigation and measurements can hopefully lead to the calculation of unit cell change with the exchange of B atoms, helping with understanding of strain build up in layers and grain boundary formation. Some work has already been done on this area [18] [17] [30]. With more extensive access to XRD and DFT calculations, a model might be constructed.

- Further devices with the 40% Sn and 60% Sn composition will hopefully show promising results in terms of stability and consistency against oxidation. I would like to see further development of these films as I am sure higher results can be achieved as the first attempts had flaws.

- FIRA was very versatile tool for annealing both ETM and Perovskite on paper, thin glass and thick devices. The future of this method looks bright.

- Pursuing epitaxial growth of mixed Sn/Pb perovskite might be the clue to using compositional addition of strain in the material to achieve single crystal thin films. Recent articles show the topic of stain created naturally in a material to be a very interesting discussion for Photovoltaics and specifically $FAPbI_3$ [32]. If one can use epitaxy and measure the strain on the surface according to Vegard's law the lattice parameters might be frugally approximated to aid in the creation of a model of the Sn/Pb unit cell upon composition change. It is very probable that the stain will differ for different alloy concentrations.

- Adding Cs to perovskite has been proved to probably prevent trap states in previous work, something that might not be relevant to Sn addition and could separately improve the mixed perovskite pin cells as long as similar morphology is still achieved [33].

References

[1] Andy Extance. Perovskites on trial, companies say they are close to commercializing a cheap photovoltaic material that could disrupt solar power — but are they too optimistic? *Nature*, 570:429–432, 2019.

[2] Piotr Kowalczewski and Lucio Claudio Andreani. Towards the efficiency limits of silicon solar cells: How thin is too thin? *Solar Energy Materials and Solar Cells*, 143:260–268, 2015.

[3] Sabre Kais Fahhad H. Alharbi. Theoretical limits of photovoltaics efficiency and possible improvements by intuitive approaches learned from photosynthesis and quantum coherence. *Renewable and Sustainable Energy Reviews*, 43:1073–1089, 2015.

[4] Feng Hao, Constantinos C. Stoumpos, Robert P. H. Chang, and Mercouri G. Kanatzidis. Anomalous band gap behavior in mixed sn and pb perovskites enables broadening of absorption spectrum in solar cells. *J. Am. Chem. Soc.*, 22:8094–8099, 2014.

[5] NREL.gov. Nrel best research-cell efficiencies official chart.

[6] Dechan Angmo, Xiaojin Peng, Aaron Seeber, Chuantian Zuo, Mei Gao, Qicheng Hou, Jian Yuan, Qi Zhang, Yi-Bing Cheng, and Doojin Vak. Controlling homogenous spherulitic crystallization for high-ef [U+FB01] ciency planar perovskite solar cells fabricated under ambient high-humidity conditions. *Small*, 15:1904422, 2019.

[7] Christopher Grote and Robert F. Berger. Strain tuning of tin–halide and lead–halide perovskites: A first-principles atomic and electronic structure study. *Phys. Chem. C*, 40:22832–22837, 2015.

[8] Yaqin Wang, Weifei.Fu, Jielin Yan, Jiehuan Chen, Weitao Yang, and Hongzheng Chen. Low-bandgap mixed tin–lead iodide perovskite with large grains for high

performance solar cells. *Journal of Materials Chemistry A*, 6:13090–13095, 2018.

[9] Qiaolei Han, Ying Wei, Renxing Lin, Zhimin Fang, Ke Xiao, Xin Luo, Shuai Gu, Jia Zhu, Liming Ding, and Hairen Tan. Low-temperature processed inorganic hole transport layer for efficient and stable mixed pb-sn low-bandgap perovskite solar cells. *Science Bulletin*, 64:1399–1401, 2019.

[10] Z Yang, Z Yu, H Wei, and al. Enhancing electron diffusion length in narrow-bandgap perovskites for efficient monolithic perovskite tandem solar cells. *Nature Communications*, 10, 2019.

[11] Wolfgang Tress Michael Saliba Stefanie Neutzner Taisuke Matsui Fabrizio Giordano T. Jesper Jacobsson Ajay Ram Srimath Kandada Shaik M. Zakeeruddin Annamaria Petrozza Antonio Abate Mohammad Khaja Nazeeruddin Michael Grätzel Juan Pablo Correa Baena, Ludmilla Steier and Anders Hagfeldt. Highly efficient planar perovskite solar cells through band alignment engineering. *(Communication) Energy Environ. Sci.*, 8:2928–2934, 2015.

[12] Reza Nekovei R.Radhakrishnan R.Jeyakumara, Atanu Bag. Interface studies by simulation on methylammonium lead iodide based planar perovskite solar cells for high efficiency. *Solar Energy*, 190:104–111, 2019.

[13] Chun-Sheng Jiang, Mengjin Yang, Yuanyuan Zhou, Bobby To, Sanjini U. Nanayakkara, Joseph M. Luther, Weilie Zhou, Joseph J. Berry, Jao van de Lagemaat, Nitin P. Padture, Kai Zhu, and Mowafak M. Al-Jassim. Carrier separation and transport in perovskite solar cells studied by nanometre-scale profiling of electrical potential. *Nature Communications*, 6:8397, 2015.

[14] The Solar Spark The University of Edinburgh in Scotland. P-n junction solar cells.

[15] Vesta. Vesta. 2019.

[16] Ke Meng, Xiao Wang, Qiaofei Xu, Zhimin Li, Zhou Liu, Longlong Wu, Youdi Hu, Ning Liu, and Gang Chen. In situ observation of crystallization dynamics and grain orientation in sequential deposition of metal halide perovskites. *Advanced Functional Materials*, 35:1902319, 2019.

[17] Constantinos C Stoumpos, Christos D. Malliakas, and Mercouri G. Kanatzidis. Semiconducting tin and lead iodide perovskites with organic cations: Phase transitions, high mobilities, and near-infrared photoluminescent properties. *Inorg. Chem.*,

52:9019–9038, 2013.

[18] Prof. Robert F. Berger. Design principles for the atomic and electronic structure of halide perovskite photovoltaic materials: Insights from computation. *Chemistry, A European Journal*, 24:8708–8716, 2018.

[19] Oleg Selig Giulia Giubertoni Huib J. Bakker Yves L. A. Rezus Jarvist M. Frost Thomas L. C. Jansen Robert Lovrincic Nathaniel P. Gallop, Nathaniel P. Gallop and Artem A. Bakulin. Theoretical limits of photovoltaics efficiency and possible improvements by intuitive approaches learned from photosynthesis and quantum coherence. *J. Phys. Chem. Lett.*, 20:5987–5997, 2018.

[20] Yunlong Li and al. 50% sn[U+2010]based planar perovskite solar cell with power conversion efficiency up to 13.6%. *Nat Energy*, 2:17018, 2016.

[21] D. Richmond, M. McCormick, T. K. Ekanayaka, J. D. Teeter, B. L. Swanson, N. Benker, G. Hao, S. Sikich, A. Enders, A. Sinitskii, C. C. Ilie, P. A. Dowben, and A. J. Yost. Inkjet printing all inorganic halide perovskite inks for photovoltaic applications. *J. Vis. Exp.*, 143:e58760, 2019.

[22] Sandy Sánchez, Xiao Hua, Antonio Günzler, Esteban Bermúdez-Ureña, Dedy Septiadi, Michael Saliba, and Ullrich Steiner. Flash infrared pulse time control of perovskite crystal nucleation and growth from solution. *Cryst. Growth Des.*, 20, 2:670–679, 2020.

[23] Ashraf Uddin, Mushfika Baishakhi Upama, Haimang Yi, and Leiping Duan. Encapsulation of organic and perovskite solar cells: A review. *Coatings*, 9(2):65, 2018.

[24] Online people directory EPFL. Sandy sanchez alonso.

[25] Eugen Zimmermann, Ka Kan Wong, Michael Müller, Hao Hu, Philipp Ehrenreich, Markus Kohlstädt, Uli Würfel, Simone Mastroianni, Gayathri Mathiazhagan, Andreas Hinsch, Tanaji P. Gujar, Mukundan Thelakkat, Thomas Pfadler, and Lukas Schmidt-Mende. Characterization of perovskite solar cells: Towards a reliable measurement protocol. *APL Materials*, 4:091901, 2016.

[26] Michael T. Postek, András E. Vladár, John S. Villarrubia, and Atsushi Muto. Comparison of electron imaging modes for dimensional measurements in the scanning electron microscope. *Microsc Microanal.*, 22(4):768–777, 2016.

[27] Brian Carlsen. Thot-data. 2020.

[28] Online people directory EPFL. Brian irving carlsen.

[29] D. Zhao, Y. Yu, C. Wang, and al. Low-bandgap mixed tin–lead iodide perovskite absorbers with long carrier lifetimes for all-perovskite tandem solar cells. *Nat Energy*, 2:17 018, 2017.

[30] Gustavo M. Dalpian, Xingang Zhao, Lawrence Kazmerski1, and Alex Zunger. Formation and composition-dependent properties of alloys of cubic halide perovskites. *Chem. Mater.*, 7:2497–2506, 2019.

[31] Sandy Sanchez, Xiao Hua, Nga Phung, Ullrich Steiner, and Antonio Abate. Flash infrared annealing for antisolvent [U+2010] free highly efficient perovskite solar cells. *Adv. Energy Mat.*, 8:1702915, 2018.

[32] Y Chen, Y Lei, and Y Li. Strain engineering and epitaxial stabilization of halide perovskites. *Nature*, 577:209—-215, 2020.

[33] Xuejie Zhu, Dong Yang, Ruixia Yang, Bin Yang, Zhou Yang, Xiaodong Ren, Jian Zhang, Jinzhi Niu, Jiangshan Feng, and Shengzhong (Frank) Liu. Superior stability for perovskite solar cells with 20% efficiency using vacuum co-evaporation. *Nanoscale*, 9:12316–12323, 2017.